Stochastic tunneling and metastable states during the somatic evolution of cancer

Peter Ashcroft [*1], Franziska Michor [†2], and Tobias Galla [‡ §1]

[1] *Theoretical Physics, School of Physics and Astronomy, The University of Manchester, Manchester M13 9PL, United Kingdom*

[2] *Department of Biostatistics and Computational Biology, Dana-Farber Cancer Institute, and Department of Biostatistics, Harvard School of Public Health, Boston, MA 02215, USA*

August 26, 2014

Abstract

Tumors initiate when a population of proliferating cells accumulates a certain number and type of genetic and/or epigenetic alterations. The population dynamics of such sequential acquisition of (epi)genetic alterations has been the topic of much investigation. The phenomenon of stochastic tunneling has been studied using a variety of computational and mathematical methods. However, the field still lacks a comprehensive analytical description; broadly speaking, theoretical predictions of fixation times are only available for cases in which the second mutant is advantageous. Here, we studied stochastic tunneling in a Moran model. Analyzing the deterministic dynamics of large populations we systematically identify the parameter regimes captured by existing approaches. Our analysis also reveals fitness landscapes and mutation rates for which finite populations have long-lived metastable states. The escape from these states is driven by intrinsic noise, and their location affects the probability of tunneling. In such situations one or both alterations are deleterious, and existing methods do not apply. For these parameter regimes we used the so-called Wentzel-Kramers-Brillouin method to compute fixation times, successfully validated by stochastic simulations. Our work fills a gap left by previous approaches and provides a more comprehensive description of the acquisition of multiple mutations in populations of somatic cells.

Keywords: stochastic modeling, population genetics, cancer, Moran process, WKB method

[*] peter.ashcroft@postgrad.manchester.ac.uk

[†] michor@jimmy.harvard.edu

[‡] tobias.galla@manchester.ac.uk

[§] Corresponding author

INTRODUCTION

Human cancer initiates when cells within a proliferating tissue accumulate a certain number and type of genetic and/or epigenetic alterations (Knudson 1971; Weinberg 2013). These alterations can be point mutations, amplification and deletion of genomic material, structural changes such as translocations, loss or gain of DNA methylation and histone modifications, and others (Weinberg 2013). The exact number and identity of these changes necessary to initiate tumorigenesis depends on the tumor type and subtype (Weinberg 2013). It is a unifying principle, however, that most cancers result from the sequential accumulation of several (epi)genetic alterations.

The dynamics of mutation acquisition is governed by evolutionary parameters such as the rate at which alterations arise, the selection effect that these alterations confer to cells, and the size of the population of cells that proliferate within a tissue. Much effort has been devoted to model these processes mathematically and computationally, and to analyze the rates at which mutations arise within pre-cancerous tissues (Nordling 1953; Armitage and Doll 1954; Fisher 1958; Moolgavkar 1978; Moolgavkar and Luebeck 1992; Nunney 1999; Gatenby and Vincent 2003; Michor *et al.* 2004; Haeno *et al.* 2009). In particular, several investigators have studied the dynamics of two mutations arising sequentially in a population of a fixed finite number of cells. For this scenario, the mean time needed for the second mutant to take over the population, known as the 'fixation time', was computed (Michor *et al.* 2004). Subsequent modeling work (Komarova *et al.* 2003; Iwasa *et al.* 2004; Nowak *et al.* 2004; Proulx 2011; Haeno *et al.* 2013) revealed a more detailed picture, in which a homogeneous population harboring no mutations can move to a homogeneous state in which all cells carry two mutations without ever visiting a homogeneous state in which all cells harbor just one mutation. This phenomenon is referred to as 'stochastic tunneling' and represents an additional route to the homogeneous state with two mutations; the sequential route is still available to the system, but it becomes less likely in certain parameter regimes.

So far, most analytical investigations of stochastic tunneling (Komarova *et al.* 2003; Iwasa *et al.* 2004; Nowak *et al.* 2004; Proulx 2011) have been limited to considering transitions between homogeneous states of the population; that is, in a system in which cells acquire two mutations, investigators focused only on states of the population in which *all* cells have either zero, one or two mutations. Sequential acquisition of mutations then corresponds to transitions from the all-0 state to the all-1 state and then to the all-2 state, while tunneling indicates transitioning from the all-0 state to the all-2 state without ever reaching the all-1 state. These investigations were performed assuming that cells proliferate according to the Moran process - a stochastic model of overlapping generations in which one cell division and one death event

occur during each time step (Moran 1962). Komarova *et al.* (2003) used this model to obtain explicit expressions for the tunneling rate when considering homogeneous states. Subsequently, Nowak *et al.* (2004) analyzed the effect of the population size and mutation rates on the rate of appearance of a single cell with two mutations. These authors noted that for small, intermediate, and large populations, it takes two hits, one hit and zero hits, respectively, for a cell to accumulate two mutations. Here a hit is defined as a rate-limiting step, such as the appearance of an alteration when mutation rates are small. Iwasa *et al.* (2004) then derived the tunneling rate for the case of a deleterious or neutral first mutant by considering the expected lineages of cells harboring one mutation. Later on, Iwasa *et al.* (2005) used the assumption of independent lineages to compute the probability distribution for the time of emergence of a single second mutant in intermediate or large populations. In this work, individual lineages of cells harboring one mutation were considered to behave independently from each other. Recently, Haeno *et al.* (2013) included the effects of large mutation rates to improve the accuracy of the tunneling rate predictions of Iwasa *et al.* (2004).

While most of the work discussed above was based on the Moran process, other types of dynamics such as the Wright-Fisher process have been studied as well, see e.g. Proulx (2011). In the Wright-Fisher process, cell generations are assumed to be non-overlapping, so that many birth and death events occur during each time step (Ewens 2004). Using this process, Weinreich and Chao (2005) determined the critical population sizes for sequential fixation or stochastic tunneling, and Weissman *et al.* (2009) calculated the rate of tunneling as a function of the mutation rates, population size, and relative fitness of cells harboring one mutation. Finally, these results were extended to investigate the effects of recombination, or sexual reproduction, on the rate of stochastic tunneling (Weissman *et al.* 2010; Lynch 2010; Altland *et al.* 2011). These authors found that the time to establishment of the double-mutant cells can be reduced by several orders of magnitude in the case of sexual reproduction when compared to the asexual reproduction case (Weissman *et al.* 2010).

The existing approaches for the Moran model provide accurate analytical approximations for a subset of the parameter space in which a cell with two mutations is advantageous compared to the other two cell types. Here we present a systematic overview of the scope of existing quantitative work. We note that there are extensive regions in parameter space which, up to date, have been left unexplored by analytical approaches. These are mostly situations in which one or both of the acquired mutations are deleterious. Before reaching fixation in the all-2 state, the population has to travel across a fitness valley or move constantly downhill in fitness space. The dynamics can then become trapped in quasi equilibria, and final fixation of a double mutant is driven purely by demographic fluctuations. We address this regime based on ideas

from mathematical statistical physics. Specifically we employ the Wentzel-Kramers-Brillouin (WKB) method (Wentzel 1926; Kramers 1926; Brillouin 1926) to derive quantitative predictions for fixation times in these parameter regimes. This method is useful for situations in which a stochastic interacting-agent system is trapped in a metastable state before it reaches final absorption. To escape the metastable state, the system has to cross a dynamic barrier separating the basin of the metastable state from the absorbing state. Examples of using the WKB method in this scenario include the computation of mixing times in evolutionary games (Black *et al.* 2012), investigating extinction processes in coexisting bacteria (Lohmar and Meerson 2011) or predator-prey systems (Gottesman and Meerson 2012), and investigating epidemic models (van Herwaarden and Grasman 1995; Kamenev and Meerson 2008; Dykman *et al.* 2008; Black and McKane 2011; Billings *et al.* 2013). In the context of stochastic tunneling, Altland *et al.* (2011) used known general results from the WKB approach to predict that the escape time increases exponentially with the population size and the depth of the fitness valley when the invading mutations are deleterious.

In this paper, we first classified the generic types of behavior that can occur in a population of cells which acquire two subsequent mutations in a Moran process: we determined when metastable states occur, when fixation is driven by intrinsic noise as opposed to deterministic flow, and where in parameter space fixation occurs in several subsequent hits. This classification was achieved by systematically studying the underlying deterministic dynamics of the process. We then obtained analytical expressions for fixation times in parameter regimes which could not be captured by previous methods, i.e. regimes in which metastable states are found. We thus employed the WKB method to provide a more complete analytical description of the fixation dynamics in these parameter regimes. Our work fills the gap left by the existing literature and leads to a more comprehensive understanding of stochastic tunneling in populations of evolving cancer cells.

THE MODEL

We considered a well-mixed, finite population of N cells (Fig. 1A). Each cell can be of one of three possible types, labeled type-0 – a wild-type cell harboring no mutations, type-1 – a cell harboring one mutation, and type-2 – a cell harboring two mutations. Initially, all cells are of type-0. The evolution of the population is determined by a Moran process (Moran 1962). During each elementary time step of this process, a cell is randomly chosen to reproduce proportional to its fitness. In the same time step another cell is randomly removed, such that the total population size remains constant. The daughter cell can either inherit its type from the parent, or acquire a mutation during division (Fig. 1A). The relative fitness values of type-0, type-1 and type-2

cells are denoted by r_0, r_1 and r_2. We use $r_0 = 1$ throughout. The mutation rates u_1 and u_2 denote the probability that the daughter of a type-0 cell is of type 1, and the probability that the daughter of a type-1 cell is of type 2, respectively. We neglect all other combinations of mutations such that, once type-0 cells become extinct, they cannot be reintroduced.

Finite populations eventually reach a state in which all cells have acquired two mutations. This state is 'absorbing', i.e. once this state has been reached, no further dynamics can occur. Any cell that is removed in this state would be replaced by a cell of type 2, so that no net change of the state of the population can occur. Depending on the parameter regimes, different paths to fixation of type-2 cells may occur. The initial mutant may take over the entire population before a second mutation arises – the system will hence reach all-1 state before cells with two mutations appear and eventually reach fixation. Alternatively, the population may reach the state in which all cells are of type 2 without ever transitioning through the state in which all cells are of type 1 – this is referred to as 'tunneling' (Fig. 1B). The term 'stochastic' indicates that, for a fixed set of parameters, either of the two routes may be taken. Which one is taken in any particular realization of the stochastic process solely depends on the specific sequence of random events in the Moran process.

Denote the number of type-0, type-1, and type-2 cells by n_0, n_1 and n_2, respectively; we have $N = n_1 + n_2 + n_3$. The transition rates for the Moran process are given by

$$\begin{aligned}
T^{1\to 0} &= \frac{(1-u_1) r_0 \frac{n_0}{N}}{\overline{r}} n_1, \\
T^{2\to 0} &= \frac{(1-u_1) r_0 \frac{n_0}{N}}{\overline{r}} n_2, \\
T^{0\to 1} &= \frac{u_1 r_0 \frac{n_0}{N} + (1-u_2) r_1 \frac{n_1}{N}}{\overline{r}} n_0, \\
T^{2\to 1} &= \frac{u_1 r_0 \frac{n_0}{N} + (1-u_2) r_1 \frac{n_1}{N}}{\overline{r}} n_2, \\
T^{0\to 2} &= \frac{u_2 r_1 \frac{n_1}{N} + r_2 \frac{n_2}{N}}{\overline{r}} n_0, \\
T^{1\to 2} &= \frac{u_2 r_1 \frac{n_1}{N} + r_2 \frac{n_2}{N}}{\overline{r}} n_1.
\end{aligned} \tag{1}$$

The quantity $\overline{r} = (r_0 n_0 + r_1 n_1 + r_2 n_2)/N$ is the average fitness in the population. The transition labeled '$i \to j$' represents a process in which a cell of type i is replaced by a cell of type j. In a process labeled '$1 \to 0$', for example, the state of the population changes from (n_0, n_1, n_2) to state $(n_0 + 1, n_1 - 1, n_2)$. As an example, the first reaction rate, $T^{1\to 0}$, in Eq. (1) can be broken down as follows: a type-0 cell is chosen to reproduce at rate $(n_0/N) \times (r_0/\overline{r})$. The offspring does not mutate with probability $(1 - u_1)$. Finally, a type-1 cell is chosen to be removed at rate

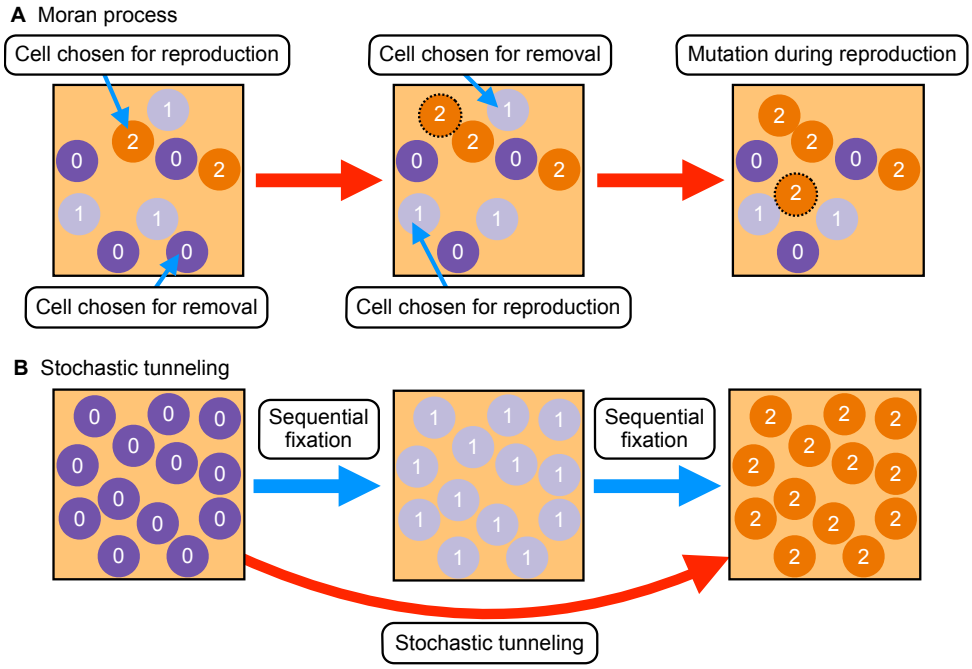

Figure 1 Moran process and illustration of tunneling. **A** Schematic of the Moran process. In the leftmost panel, a type-0 cell is chosen for removal, and a type-2 cell is chosen to reproduce. In the next step (center) a type-1 cell is chosen for removal, and another type-1 cell for reproduction. In the rightmost panel this change is implemented, however a mutation occurs during the reproduction such that the offspring of the reproducing type-1 cell is of type 2. **B** Schematic illustration of stochastic tunneling. The population can reach the all-2 state via two routes. The first is the sequential fixation route in which the first mutation takes over the population, and where this is then followed by the second mutation. The second route does not visit the all-1 state. This is the stochastic tunneling route.

n_1. The rates for the other processes can be interpreted analogously. We choose a continuous-time setup, and correspondingly all rates in Eq. (1) scale linearly in the population size N. Simulations are carried out using a standard Gillespie algorithm (Gillespie 1977).

This process is described exactly by a master equation (Van Kampen 2007), which governs the behavior of the probability, $P_{\vec{n}}(t)$, that the population is in state $\vec{n} = (n_0, n_1, n_2)$ at time t, and is given by

$$\dot{P}_{\vec{n}}(t) = \sum_{\vec{v}} \left[T^{\vec{v}}_{\vec{n}-\vec{v}} P_{\vec{n}-\vec{v}}(t) - T^{\vec{v}}_{\vec{n}} P_{\vec{n}}(t) \right]. \tag{2}$$

The vector $\vec{v}$ indicates a change in the composition of the population due to the corresponding reaction, and $\dot{P}_{\vec{n}}(t)$ represents the partial derivative of $P_{\vec{n}}(t)$ with respect to time. This equation states that the probability that the population is in state $\vec{n}$ at time t increases due to transitions into the state $\vec{n}$ and decreases due to transitions out of the state $\vec{n}$.

The master equation contains full information about the stochastic population dynamics. In particular, the detailed statistics of the population at any time can be derived from it, and it captures effects driven by intrinsic noise, such as extinction and fixation. Obtaining a full solution of the master equation is difficult or impossible though in all but the simplest of cases. As a starting point, it is often useful to first consider the deterministic limit of infinite populations. In this limit, the distribution $P_{\vec{n}}(t)$ is sharply peaked around its average, and so the dynamics reduces to a set of equations for this mean. This approach does not capture any of the stochastic effects. However, the types of stochastic trajectories that can be observed for different parameter sets are, to some extent, set by the underlying deterministic dynamics. We thus first analyze the deterministic limit of the model.

DETERMINISTIC ANALYSIS AND TYPES OF STOCHASTIC BEHAVIOR

In the limit $N \to \infty$, the population evolves according to a deterministic set of equations. Writing $x_i = \lim_{N\to\infty} n_i/N$, we have the relation $x_0 + x_1 + x_2 = 1$, and the average fitness is given by $\overline{r} = r_0 x_0 + r_1 x_1 + r_2 x_2$. The equations governing the dynamics of the population are then

$$\begin{aligned} \overline{r}\dot{x}_0 &= \big[(1-u_1)r_0 - \overline{r}\big]x_0, \\ \overline{r}\dot{x}_1 &= u_1 r_0 x_0 + \big[(1-u_2)r_1 - \overline{r}\big]x_1, \\ \overline{r}\dot{x}_2 &= u_2 r_1 x_1 + (r_2 - \overline{r})x_2. \end{aligned} \tag{3}$$

These equations can be derived systematically using a system-size expansion of the master equation (2), see e.g. Van Kampen (2007). Note that x_i refers to the relative concentration

of cells of type i in the population (not to be confused with the probability of being found in a homogeneous state of type-i cells as studied in (Iwasa *et al.* 2004; Haeno *et al.* 2013)). For example, $x_0 = x_1 = x_2 = 1/3$ would indicate that the population is in a state in which all three types are present with equal numbers.

Given the relation $x_0 + x_1 + x_2 = 1$, the dynamics only has two independent degrees of freedom. Time courses of the system can hence be thought of as a trajectory in a 'concentration simplex', as depicted in the satellite diagrams of Fig. 2. Each point in the simplex represents one particular state $(1 - x_1 - x_2, x_1, x_2)$ of the population. At points in the interior of the simplex all three types of cells are present in the population ($x_i > 0$ for $i = 1, 2, 3$). Points on the edges of the simplex represent states in which one of the three types is not present, for example $x_0 = 0$ for points along the edge connecting the lower-right corner of the simplex with the upper corner. We will refer to this as the 1–2 edge in the following, and similarly for the other edges. The three corners of the simplex represent points at which all cells are of the same type, i.e. $x_0 = 1$ (lower left corner), $x_1 = 1$ (lower right) and $x_2 = 1$ (upper corner).

The deterministic equations (3) can have zero, one, or two fixed points (FP) depending on the values of the fitness parameters and the mutation rates. Mathematically these fixed points are defined as points $(1 - x_1^* - x_2^*, x_1^*, x_2^*)$ at which $\dot{x}_i = 0$ for all $i = 0, 1, 2$. Each fixed point can either be stable (i.e. attracting from all directions) or a saddle (attracting from some directions, repelling in others). The system is found not to contain any fully repelling fixed points (Appendix A). Fig. 2 shows the deterministic dynamics in different parameter regimes, indicated as Regions I to V. Below we discuss the stochastic behavior in each of these parameter regimes.

Region I (stable fixed point on the 1–2 boundary):
In Region I, the deterministic dynamics flows towards a fixed point on the 1–2 edge of the concentration simplex, i.e. a fixed point at which there are no cells of type 0 ($x_0 = 0$). The deterministic system gets stuck at this fixed point, but a finite population still eventually reaches fixation in the all-2 state. At large but finite population sizes, the stochastic dynamics are expected to approximately follow the deterministic path shown in Fig. 2. Cells of type 0 will quickly become extinct, and the system reaches the 1–2 edge. The lack of backwards mutations means the population cannot depart from this edge, and so the problem becomes one-dimensional. The intrinsic noise then has to drive the system into the absorbing upper corner of the concentration simplex ($\vec{x} = (0, 0, 1)$) against the deterministic flow which is towards the non-trivial fixed point on the 1–2 edge. Fixation is driven by noise and we expect fixation times to grow exponentially with the population size (Antal and Scheuring 2006; Mobilia 2010; Altland *et al.* 2011).

Region II (stable interior fixed point and saddle point on the 1–2 edge):

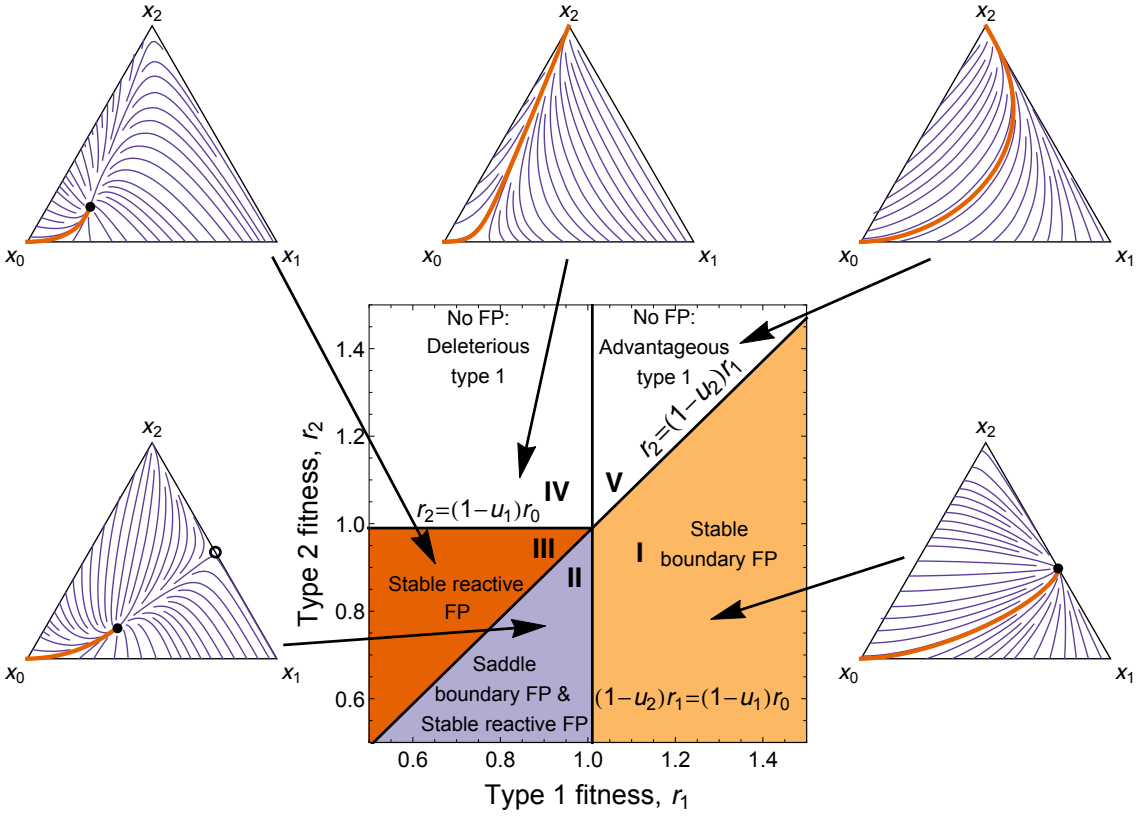

Figure 2 Phase diagram with satellite diagrams showing the deterministic flow. Fixed points are found on the 1–2 boundary and/or in the interior of the simplex. Boundary fixed points occur when $r_2 < (1-u_2)r_1$ (Regions I and II). Reactive fixed points occur when $r_2 < (1-u_1)r_0$ and $(1-u_2)r_1 < (1-u_1)r_0$ (Regions II and III). No fixed points are found in Regions IV and V. The satellite diagrams show the deterministic flow, Eq. (3). Thick (red) lines show the deterministic flow from the all-wild-type initial condition. Solid circles indicate stable fixed points, and the empty circle for Region II corresponds to a saddle point which is stable along the 1–2 boundary. In all cases, the point $x_2 = 1$ is an absorbing state and is therefore a fixed point as well.

In Region II, the deterministic flow from the all-wild-type state is towards a stable fixed point in the interior of the simplex. This fixed point is referred to as the 'reactive' fixed point in-line with previous literature (Rulands *et al.* 2013). The deterministic system has a second fixed point on the 1–2 edge. The deterministic flow *on* this edge is towards this second fixed point. However, at a small distance away from the edge the flow is directed towards the reactive fixed point. Thus, the fixed point on the edge is a saddle (stable along the edge, unstable in directions away from the edge). As before the stochastic dynamics in finite populations will reach the all-2 state eventually. Initially the system evolves close to the deterministic trajectory (see Fig. 2) and then gets 'trapped' near the reactive fixed point. The population will fluctuate about this fixed point until it eventually overcomes the deterministic flow and escapes. There are two possibilities for the subsequent behavior: (i) Cells of type 0 become extinct first due to the stochastic nature of the dynamics. The population then becomes trapped on the 1–2 edge. It will fluctuate about the fixed point on this edge until further fluctuations enable the system to overcome the deterministic flow and to reach the absorbing upper corner of the concentration simplex. This corresponds to sequential extinction, first of type-0 cells, then of type-1 cells. A trajectory of this type is illustrated in Figs. 3A and 3C; (ii) Cells of type 0 and type 1 can in principle go extinct (almost) simultaneously. The trajectory of the system then hits the 1–2 edge infinitesimally close to the all-2 corner of the simplex (here 'infinitesimally close' means a distance of order $1/N$ away from the upper corner). In numerical simulations (data not shown) we find that this second path is realized only very rarely, and so our mathematical analysis of Region II below focuses on sequential extinction.

Region III (stable interior fixed point):
In Region III the deterministic dynamics has a single stable fixed point in the interior of the concentration simplex. Large, but finite populations will behave as discussed in case (ii) for Region II. They will initially become trapped near the reactive fixed point, before fluctuations eventually push the system to the absorbing state at the all-2 corner of the concentration simplex. In Region III, type-0 cells and type-1 cells essentially go extinct at the same time. If the type-0 cells become extinct first, the deterministic flow along the 1–2 edge is directed towards the absorbing state such that type-1 cells quickly become extinct. This is illustrated in Figs. 3B and 3D.

Regions IV and V (no fixed points other than the absorbing all-2 state:
In a subset of the parameter space, shown as Regions IV and V in Fig. 2, the deterministic flow from the $\vec{x} = (1, 0, 0)$ state is directly to the absorbing state $\vec{x} = (0, 0, 1)$. For such model parameters we expect that fixation in finite populations will be quick as the deterministic flow promotes fixation.

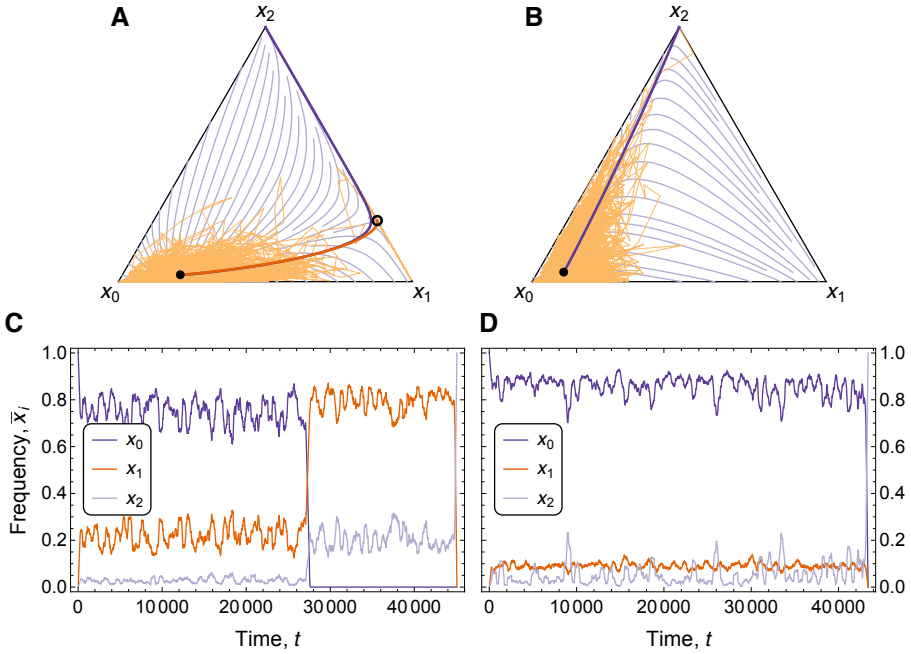

Figure 3 Routes to fixation in cases with a fixed point in the interior of the concentration simplex. **A** The concentration simplex for a combination of parameters in Region II ($r_1 = 0.96$, $r_2 = 0.91$, $u_1 = 0.01$, $u_2 = 0.01$). The red line is the dominant path for sequential extinction, as obtained from the WKB analysis (see text). The thick purple line indicates the dominant path for simultaneous extinction of types 0 and 1, which is rare. Thin lines indicate the deterministic flow [Eq. (3)]. The orange line represents the trajectory of a single stochastic simulation ($N = 300$). **B** Dominant trajectory, flow lines, and stochastic trajectory for a combination of parameters in Region III ($r_1 = 0.90$, $r_2 = 0.97$, $u_1 = 0.01$, $u_2 = 0.01$). Cells of types 0 and 1 go extinct (essentially) at the same time $t \approx 44,000$. The dominant trajectory as obtained from the WKB calculation (thick purple line) runs directly into the all-2 corner of the concentration simplex. **C** The concentrations of the three types of cells as a function of time. These are obtained from the same stochastic simulation as shown in the simplex **A**. A moving average has been taken to improve clarity. As seen from the data cells go extinct sequentially: initially all three types are present, cells of type 0 go extinct at time $t \approx 28,000$, cells of type 1 go extinct at time $t \approx 45,000$. **D** The concentrations (moving average) of the three types of cells as a function of time for the stochastic simulation shown in the simplex **B**.

Fig. 4 illustrates which parameter regimes have previously been studied in the literature. These existing studies almost exclusively focus on Regions IV and V in Fig. 2, i.e. on cases in which fixation is driven not primarily by demographic noise, but by the underlying deterministic flow. Large populations can be expected to closely follow the deterministic trajectory, and so there is tunneling. Smaller populations may well hit the all-1 corner along the way, so they may show sequential fixation without tunneling. As mentioned above fixation is typically fast in Regions IV and V. Based on similar studies in evolutionary game theory one would expect the fixation time to grow logarithmically with the population size, $\tau \sim \ln N$ (Antal and Scheuring 2006), and this is indeed what we find in simulations (data not shown). The regions containing non-trivial fixed points are largely unexplored by previous investigations. In these parameter regimes the deterministic flow reaches a fixed point away from the absorbing state. Therefore, fixation is controlled by stochastic effects so that fixation times are large and broadly distributed. As we will discuss below, fixation times grow exponentially with the population size in such cases. This is perfectly in-line with the findings of Haeno *et al.* (2013), who point out that fixation in these regions takes a very long time. Efficient measurements of fixation time in simulations are hence difficult. Methods which require the numerical solutions of, for example, the backward Fokker-Planck equation or a backward master equation reach their limits here as well (Haeno *et al.* 2013). The contribution of our work is to analyze precisely these previously inaccessible cases. We compute the fixation properties of systems in which the underlying deterministic flow has one or more attracting fixed points away from the absorbing all-2 state.

WKB ANALYSIS

Let us now analyze the dynamics in Regions I, II and III, i.e. in situations in which the deterministic dynamics has one or several non-trivial fixed points, generating long-lived metastable states for finite populations. The WKB method is based on the assumption that the population quickly reaches the vicinity of such a metastable state. From this state, stochastic fluctuations push the population to the absorbing state, $\vec{n}_{abs}$, on a very long timescale $\tau \gg t_r$, where t_r is the relaxation timescale to the metastable state (Assaf and Meerson 2010). This approach is known as the quasi-stationary approximation. Making these assumptions we write the probability to find the population in state $\vec{n}$ as

$$P_{\vec{n}\neq\vec{n}_{abs}}(t \gg t_r) \simeq \pi_{\vec{n}}\, e^{-t/\tau}, \quad P_{\vec{n}_{abs}}(t \gg t_r) \simeq 1 - e^{-t/\tau}. \tag{4}$$

The distribution $\pi_{\vec{n}}$ is the so-called 'quasi-stationary distribution' (QSD) and describes the population in the metastable state before the absorption process sets in. This distribution is peaked about the metastable state, marked by an underlying fixed point. The exponential decay

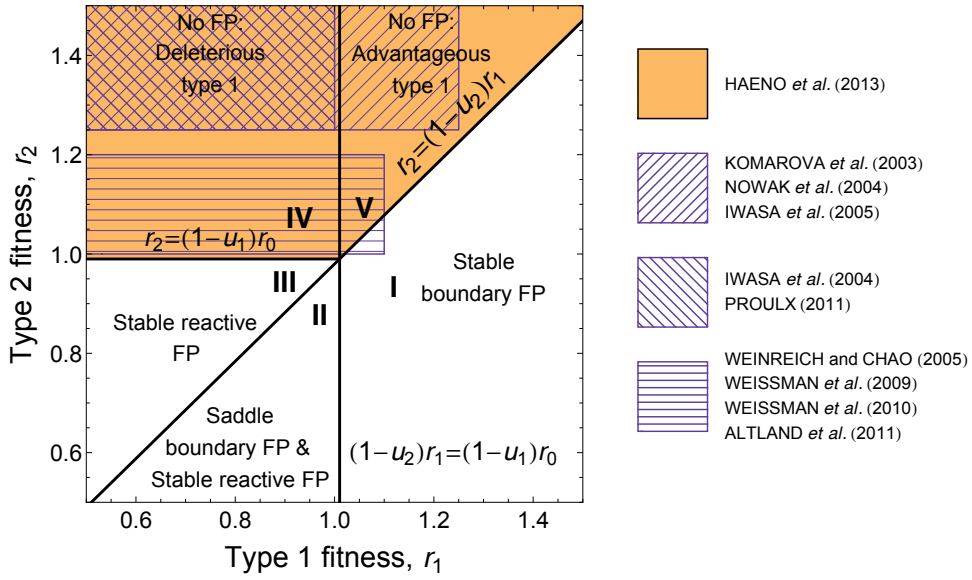

Figure 4 Phase diagram highlighting previous work. The colored area roughly corresponds to the regions in HAENO *et al.* (2013) in which the fixation probability is successfully predicted (See Fig. 6 in HAENO *et al.* (2013)). The southwest-northeast striped region, with r_1 deleterious or slightly advantageous, and r_2 very advantageous, has been studied in KOMAROVA *et al.* (2003), NOWAK *et al.* (2004), and IWASA *et al.* (2005). The northwest-southeast striped region, with r_1 neutral or deleterious, and r_2 very advantageous, has been studied in IWASA *et al.* (2004), and PROULX (2011). Finally, the horizontal striped region corresponds to the literature of crossing fitness valleys, notably WEINREICH and CHAO (2005), WEISSMAN *et al.* (2009), WEISSMAN *et al.* (2010), LYNCH (2010), and ALTLAND *et al.* (2011).

factor, $e^{-t/\tau}$, describes a slow 'leaking' process from the metastable state into the absorbing state, $\vec{n}_{abs} = (0, 0, N)$. The probability that the population has reached the all-2 state by time t is hence given by $P_{\vec{n}_{abs}}(t \gg t_r) \simeq 1 - e^{-t/\tau}$, and the mean time to reach this state is τ. The purpose of the calculation that follows is to determine the mean fixation time τ.

As a next step we use the WKB ansatz for the QSD,

$$\pi_{N\vec{x}} = \psi(\vec{x}) = e^{-NS(\vec{x})-S_1(\vec{x})}, \tag{5}$$

where $S(\vec{x})$ is a quantity known as the *action*, and $\exp[-S_1(\vec{x})]$ is the so-called 'amplitude' (Assaf and Meerson 2010). We have written $\vec{x} = \vec{n}/N$.

To find the mean fixation time of the type-2 cells, we substitute the approximation (4) into the master equation (2) to obtain the quasi-stationary master equation (QSME)

$$0 \approx -\frac{1}{\tau}\pi_{\vec{n}\neq\vec{n}_{abs}} = \sum_{\vec{v}} T^{\vec{v}}_{\vec{n}-\vec{v}}\pi_{\vec{n}-\vec{v}} - T^{\vec{v}}_{\vec{n}}\pi_{\vec{n}}. \tag{6}$$

For $\vec{n} = \vec{n}_{abs}$ (the absorbing state) we have

$$\frac{1}{\tau} = \sum_{\vec{v}} T^{\vec{v}}_{\vec{n}_{abs}-\vec{v}}\pi_{\vec{n}_{abs}-\vec{v}}, \tag{7}$$

where we have used $T^{\vec{v}}_{\vec{n}_{abs}} = 0$. Hence if we find the QSD $\pi_{\vec{n}}$ by solving the QSME (6), we can determine the mean fixation time, τ, and the probability to have reached fixation by time t, $P_{\vec{n}_{abs}}(t) = 1 - e^{-t/\tau}$.

To find the QSD, we follow e.g. Assaf and Meerson (2010) and expand the QSME (6) in powers of N^{-1}. Hence this approach is only valid for large system sizes. The further analysis can be carried out analytically for one-dimensional systems, i.e. for escape from attracting fixed points on the edges of the concentration simplex in our model. This is relevant in Regions I and II. Escape from a reactive fixed point, at which all three types of cells are present, can also be studied using the WKB ansatz. The system then retains two degrees of freedom, and the analysis must be carried out numerically. In the following we briefly describe the main steps for each of the two situations.

Analytical solution for Region I: We first consider parameter Region I in Fig. 2, in which there exists a single stable fixed point located on the 1–2 boundary of the concentration simplex. Under the quasi-stationary assumption, the population quickly reaches the vicinity of this fixed point. As the population cannot depart from the 1–2 boundary, the system then reduces to a

one-dimensional model. We parameterized the system in terms of n_1, such that $n_1 = 0$ is the absorbing state (all cells of type 2) and $n_2 = N - n_1$. The analysis now closely follows the work of Assaf and Meerson (2010), specifically their scenario A. The outcome of the analysis are expressions for the action $S(x_1)$, $S_1(x_1)$ (determined up to an additive constant), and the normalization of the QSD (5). With this we find an expression for the mean fixation time, τ, of the type-2 cells. This analysis is covered in detail in Appendix B, we here only list the main steps and the result of the solution procedure:

(i) Substitute the approximation (4) into the master equation (2) to obtain the QSME (6), and then expand in powers of N^{-1}. At leading order one recovers a Hamilton-Jacobi equation which can be solved to find the minimum value of the action $S(x_1)$. This corresponds to the most likely trajectory from the fixed point to the absorbing state (Assaf and Meerson 2010; Kamenev 2011). The equation at next-leading order can be solved to find the function $S_1(x_1)$. These expressions are obtained up to undetermined additive constants, relating to the overall normalisation of the QSD. These constants are fixed and the QSD (5) normalized by considering a Gaussian approximation of $\psi(x_1)$ about the fixed point.

(ii) Find a so-called boundary-layer solution by recursively solving the QSME (6) for $0 < n_1 \lesssim N^{1/2}$, using Eq. (7) to express the solution as a function of the expected fixation time τ.

(iii) Matching the recursive boundary-layer solution and the WKB solution in the domain $0 < n_1 < N^{1/2}$ gives the expected fixation time,

$$\begin{aligned} \tau &= \sqrt{\frac{2\pi r_1 r_2}{N u_2}} \frac{(1-u_2)(r_1-r_2)}{[(1-u_2)r_1 - r_2]^2} \\ &\quad \times \exp\left\{ N \left[\frac{u_2 r_1}{r_2 - u_2 r_1} \ln\left(\frac{u_2(1-u_2) r_1^2}{r_1 - r_2} \right) + \ln\big((1-u_2)r_1\big) - \frac{r_2}{r_2 - u_2 r_1} \ln r_2 \right] \right\} \end{aligned} \tag{8}$$

Numerical solution for Regions II and III: When a fixed point exists away from the state-space boundaries, as found in Regions II and III in Fig. 2, the solution procedure described above is no longer viable; the Hamiltonian equations recovered from step (i) above can no longer be integrated directly subject to the appropriate boundary conditions (see Appendix C). Instead, minimum-action trajectories have to be found numerically. Problems of this type are usually tackled in one of two ways: firstly, the equations of motion could be integrated using a shooting method to find the optimal (most likely) trajectory with a given final point (Kamenev and Meerson 2008; Black and McKane 2011; Gottesman and Meerson 2012); secondly, the equations can be integrated using an iterative scheme which converges to the optimal trajectory (Lohmar and Meerson 2011) connecting given start and end points. We found that the second

method quickly converges for our problem, so results presented in the following use this method. The details of the procedure are described in Appendix C.

Using this method we calculated the action, S, accumulated over the trajectory from the stable reactive fixed point to the boundary saddle fixed point in Region II, or directly to the absorbing state, $\vec{x} = (0, 0, 1)$, in Region III. We then used a known result presented by van Herwaarden and Grasman (1995) for the escape time from a metastable state,

$$\tau \sim \frac{C}{\sqrt{N}} e^{NS}, \tag{9}$$

where the constant C can be found by fitting to simulation data. This expression has the same functional dependence on N as the one given in Eq. (8).

RESULTS

Let us analyze the results separately for each region of parameter space. In particular we discuss the implications the model parameters have for the probability with which tunneling occurs, and for the fixation time of type-2 cells.

Region I: In this region, type-1 cells have a fitness advantage over both type-0 and type-2 cells, such that the fitness landscape has an intermediate maximum (a fitness 'hill'). As a result, the population quickly approaches the metastable state with a large proportion of type-1 cells while the type-0 cells become extinct. It then relaxes to the QSD on the 1–2 edge, as described above, and probability slowly leaks into the all-2 corner.

To test the accuracy of this approach, we compare the QSD measured in simulations with the theoretical approximation (Fig. 5). The data in the figure reveals good agreement between theory and computer experiment for $N^{1/2} \lesssim n_1 \leq N$, and for $n_1 = 0$. In the region just above $n_1 = 0$ the agreement between the theoretical result for P_{n_1} and simulation data breaks down; here the theoretical value diverges. This is a result of taking the limit $1/\tau \to 0$ in the QSME (6), in particular for the case $n_1 = 0$ which corresponds to $1/\tau = T^{1\to 2}_{(0,1,N-1)}\pi_1$. The value of τ is crucial to determining the value of π_1. When calculating the mean fixation time, τ, we circumvented this known problem by considering a so-called 'boundary-layer' approach (Assaf and Meerson 2010). The boundary-layer solutions (dashed lines in Fig. 5; for details of the calculation see Appendix B) show better agreement with simulation results close to $n_1 = 0$ than the QSD obtained from the WKB ansatz (solid lines).

Increasing the fitness advantage of type-1 cells over type-2 cells moves the fixed point on the 1–2

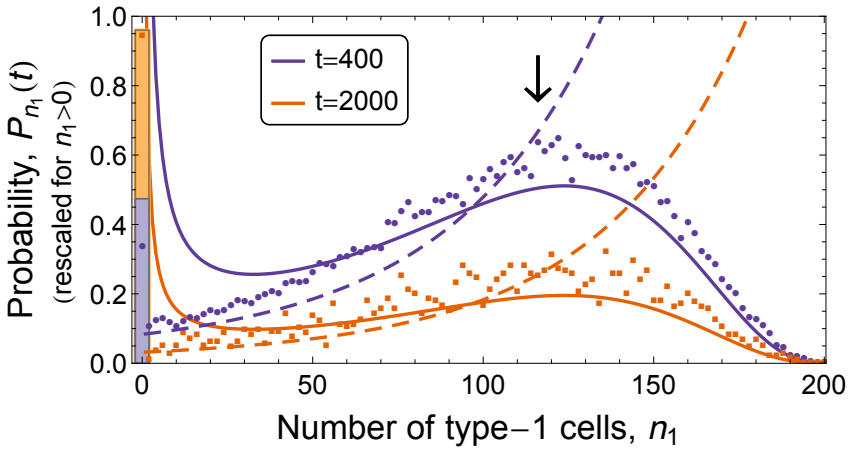

Figure 5 Quasi-stationary distribution and simulation results. We show the approximation Eq. (4) (solid lines; filled bars for $n_1 = 0$) against the distribution of states n_1 obtained from an ensemble of 10^5 simulation runs (symbols). Here the metastable state is located along the 1–2 boundary (Region I: here the solution is obtained analytically with $S(x_1)$ and $S_1(x_1)$ given by Eq. (B7), and the WKB ansatz Eq. (5) is normalized analytically by considering a Gaussian approximation about the fixed point). Dashed lines correspond to the boundary-layer solution of the master equation, valid for $0 \lesssim n_1 < N^{1/2}$ [Eq. (B11)]. Note that the distributions away from $n_1 = 0$ have been re-scaled by factors of 100 for $t = 400$ and 500 for $t = 2000$ for optical convenience. The arrow indicates the location of the fixed point. Parameters are $r_0 = 1.0$, $r_1 = 1.05$, $r_2 = 1.0$, $u_1 = 1 \times 10^{-2}$, $u_2 = 2 \times 10^{-2}$, $N = 200$.

edge closer to the $n_1 = N$ state. The probability of reaching the all-1 state due to fluctuations increases with r_1. Thus increasing the fitness advantage of type-1 cells, or likewise reducing the mutation rate u_2, will reduce the tunneling rate. We also expect the mean fixation time of type-2 cells to increase as the fixed point moves closer to the $n_1 = N$ state. This is shown in Fig. 6A, where τ is seen to increase exponentially with r_1. This slowing down of fixation reflects the increasing height of the fitness 'barrier' which must be overcome for type-2 cells to reach fixation in a mixed type-1/type-2 population. Increasing the fitness of type-2 cells, r_2, on the other hand reduces the advantage of type-1 cells and moves the fixed point closer to the all-2 absorbing state. This leads to a significant reduction in the fixation time as also shown in Fig. 6A. Reducing the mutation rate has a similar effect to reducing r_2; the fixed point moves away from the absorbing state, and selection away from the absorbing state is stronger, leading to an increase in the fixation time.

In Fig. 6B, we plot the probability that type-2 cells have reached fixation by time $t = 10^4$ (including fixation earlier than that). The data shows that this probability decreases exponentially with increasing fitness advantage of type-1 cells. Increasing r_1 leads to stronger selection away from the absorbing all-2 state, and so the population is more likely to remain close to the fixed point on the 1–2 edge. This fixed point moves away from the all-2 state as the fitness r_1 is increased, and so it becomes increasingly rare for fluctuations to drive the population to fixation at the upper corner of the concentration simplex.

In both panels of Fig. 6 the predictions for the mean fixation time of type-2 cells, Eq. (8), and for the probability to have reached fixation by a given time, Eq. (4), are in excellent agreement with simulation results. This is the case even at the relatively small population size of $N = 100$. Small deviations occur when mutations rates are low, see the dashed lines and open symbols in Fig. 6. The theory then slightly underestimates the fixation time and overestimates the probability of reaching fixation before a fixed time. This is a consequence of assuming that the population approaches the metastable state in a negligible amount of time. For very small mutation rates, it takes an increasing period of time until the mutations first appear. Deviations between theory and simulation results occur when $(1 - u_2)r_1 \simeq r_2$. At this point the theory breaks down as the fixed point on the 1–2 edge approaches the absorbing state, $\vec{x} = (0, 0, 1)$. The barrier associated with selection is then negligible, such that the assumptions underlying the WKB-approximation are no longer justified.

Region II: In this region the wild-type cells are the fittest cell type, and type-1 cells are fitter than type-2 cells. The population first approaches a stable fixed point close to the all-wild-type state. From here there are two possible routes to fixation, sequential or (almost) simultaneous

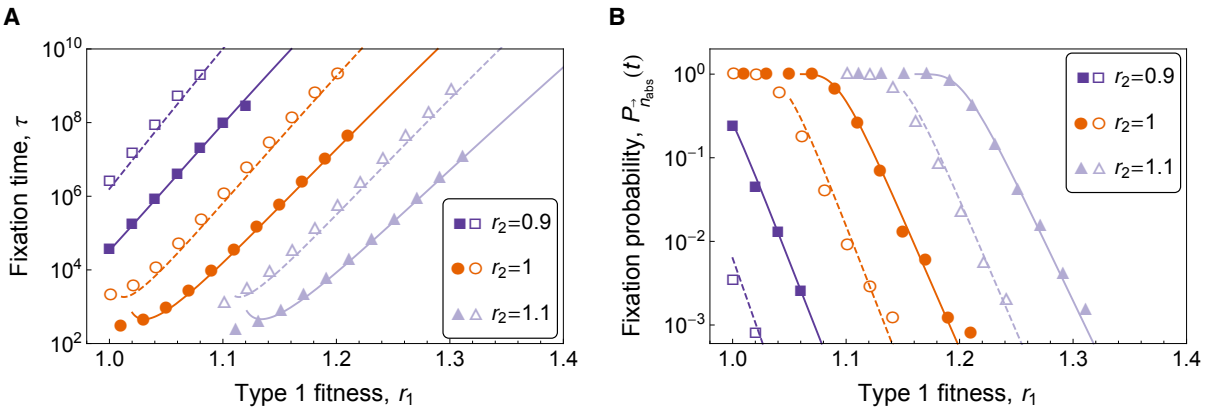

Figure 6 Results for Region I. A Mean fixation time of type-2 cells in Region I. Symbols correspond to mean fixation time from simulations of the model (averaged over an ensemble of 2–5×10^3 samples) initiated in the all-wild-type state. Shape of symbol indicates fitness of type-2 cells (see legend); filled symbols are for $u_1 = u_2 = 10^{-2}$, empty symbols are for $u_1 = u_2 = 10^{-3}$. Solid lines (high mutation) and dashed lines (low mutation) are the WKB prediction for fixation time, Eq. (8). The approximation breaks down when $(1 - u_2)r_1 \simeq r_2$, which is when the fixed point approaches the absorbing state. **B** Fixation probability of type-2 cells in Region I, evaluated at time $t = 10^4$. Lines correspond to the WKB prediction Eqs. (4) and (8), and colors and symbols follow the same convention as **A**. Remaining parameters are $r_0 = 1.0$ and $N = 100$.

extinction of types 0 and 1, as described previously and shown in Fig. 3. By computing the action accumulated along both routes, we have shown that the path of least action – the most probable path to fixation – corresponds to the path of sequential extinction. We treat this as two separate problems: (i) escape from the stable reactive fixed point (all three types present) to the boundary saddle point (mixed population of type-1/type-2 cells), and (ii) escape from the fixed point on the 1–2 edge to the absorbing all-2 state. In this two-hit process the population first fluctuates about a stable, mixed concentration of all three types before fluctuations lead to the extinction of the wild-type. The system then settles near the 1–2 equilibrium, and then type-1 cells become extinct eventually. A typical realization of this sequence of events is shown in Fig. 3C.

As in Region I, the probability of tunneling decreases as the fitness advantage of type-1 cells over type-2 cells increases. This is because the fixed point on the 1–2 edge approaches the $n_1 = N$ state. For the same reason, the tunneling rate decreases as the mutation rates decrease.

Following the convention used by Gottesman and Meerson (2012), we labeled the time to reach the boundary saddle point as τ_{32}, indicating that the 3-species system turns into a 2-species system when the wild type goes extinct. Similarly, the time to travel from the boundary fixed point (2 species present in the population) to the absorbing state (1 species) is denoted by τ_{21}. With this notation we also labeled the action accumulated along each segment as S_{32} and

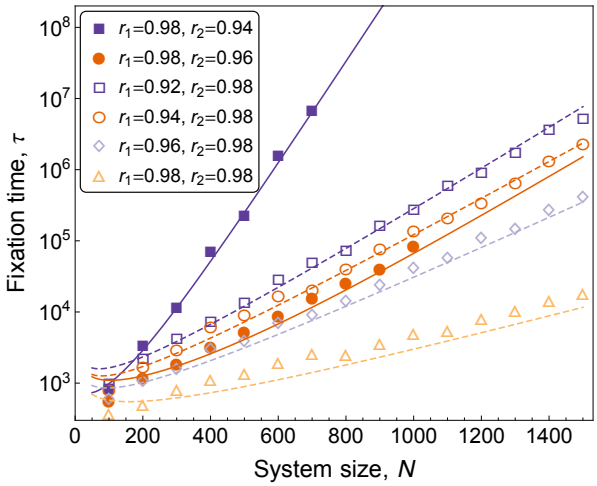

Figure 7 Results for Regions II and III. Fixation time in Region II (filled symbols) and Region III (empty symbols) of Fig. 2 as a function of system size from simulations, averaged over 100 realizations. Theory lines are of the form shown in Eq. (10) for Region II parameters (solid lines) and Eq. (9) for Region III parameters (dashed lines). Remaining parameters are $r_0 = 1.0$ and $u_1 = u_2 = 10^{-2}$.

S_{21}. As τ_{21} is given by Eq. (8), we express the mean fixation time of type-2 cells as

$$\tau = \frac{C_{32}}{\sqrt{N}} e^{NS_{32}} + \tau_{21}. \tag{10}$$

The coefficient C_{32} is found by fitting to simulation data for the time taken to reach the 1–2 boundary as a function of the population size.

Small changes to the parameters now have significant effects on the fixation time, as shown in Fig. 7 (filled symbols/solid lines). Increasing the fitness of the type-2 cells moves both the reactive fixed point and the fixed point on the 1–2 edge towards the absorbing all-2 state. It also reduces the strength of selection away from the absorbing state. These combined effects dramatically reduce the mean fixation time, and its rate of increase with the population size.

Region III: In this region the wild-type cells are again the fittest cell type, but type-2 cells now carry a higher fitness than type-1 cells. Selection along the 1–2 boundary is directed towards the absorbing all-2 state. The stable three-species state of the reactive fixed point is located close to the all-wild-type state. The dominant path to fixation of type-2 cells is directly from this state to the absorbing all-2 state, as shown in Fig. 3B. As a result the probability of tunneling is higher than in the previous cases. It increases as the fitness of type-2 cells, r_2, and the mutation rates increase as the stable state moves to lower numbers of type-1 cells.

The fixation time is computed from Eq. (9), where $S = S_{31}$ is the action accumulated along the direct path from the reactive fixed point to the all-2 state. The coefficient C is again found by fitting to simulation data. We see in Fig. 7 (empty symbols/dashed lines) that varying the model parameters has a lesser effect on fixation times that in Region II. In Region III, fixation is a one-hit process – the population only has to escape the stable fixed point – and not a two-hit process as in Region II where the effects of the two steps are compounded. Contrary to the results for Region I, the mean fixation time is a decreasing function of r_1 in Region III. This can be explained as follows: by increasing r_1, the selection strength away from the 1–2 boundary decreases and the stable state moves to higher type-1 numbers, such that the population has an improved chance of reaching the 1–2 boundary. From there selection is directed towards the absorbing state, and the time spent on the 1–2 boundary is negligible compared to the time to reach this edge. Hence, the fixation time reduces as type-1 cells become more fit. The rate of increase of the fixation time with the population size reduces as well (see Fig. 7).

Note that there are systematic deviations between theory and simulation results in data set shown as open triangles in Fig. 7, and to a lesser extent also for the data shown as open diamonds. This is attributed to the fact that the fitness parameters r_1 and r_2 are very similar to each other or equal for these instances, and they are also close to the fitness of the wild-type. Selection is then close neutral and the metastable state is only weakly attracting. The WKB approach then reaches its limits, as the assumption of a long-lived metastable state begins to break down.

DISCUSSION

In this paper, we investigated the fixation of two successive mutations in a finite population of cells proliferating according to the Moran process. We first analyzed the underlying deterministic dynamics, formally valid in the limit of an infinitely large population. In this case the population is described by a set of coupled ordinary differential equations for the proportion of cells with zero, one and two mutations, respectively. A detailed analysis of the fixed points of this system allowed us to systematize the different types of dynamic scenarios one might expect for the stochastic system. We were thus able to divide parameter space into distinct regions – those without non-trivial fixed points, those with one fixed point, and those with two fixed points. Stable fixed points of the deterministic dynamics translate into long-lived metastable states for the stochastic dynamics of finite populations. Our analysis identified the escape from these metastable states as the key bottleneck to fixation of cells with two mutations. For parameter values for which there are no deterministic fixed points the fixation dynamics is largely governed by the deterministic flow. The rate-limiting steps are then the appearance of the first mutant of

each type (Nowak *et al.* 2004), and the subsequent fixation of cells with two mutations is a zero-hit process. If there is one stable fixed point, then the process becomes a one-hit phenomenon, limited by the escape from this metastable state. In regions with two fixed points one observes a two-hit process. The population becomes trapped in a first metastable state, escapes to a second metastable state, and then reaches full fixation. In terms of the development of tumors, our analysis shows that the path to accumulating mutations can be complex and is not simply limited by the mutation rates, but also by escape from metastable states. Populations can exist in a heterogeneous state for very long periods of time before fluctuations eventually drive the second mutants to fixation. The probability with which stochastic tunneling occurs is, in part, determined by the location of these metastable states.

In addition to systematically classifying the qualitative behavior of the population dynamics, we also calculated fixation times in parameter regimes previously inaccessible to existing analytical approaches. These are precisely the regions of parameter space in which metastable states are found. We used the Wentzel-Kramers-Brillouin (WKB) approximation to calculate the long-lived quasi-stationary states of the population and the mean time it takes to reach fixation in a state in which all cells have acquired two mutations. Based on this approach, we classified how changing the fitness landscape and mutation rates affects the rate of stochastic tunneling and the time-to-fixation of the cells harboring two mutations. When cells with one mutation are fitter than those with two mutations, the probability of tunneling is low, and it decreases as the fitness gap between these two types of cells increases or as mutation rates decrease. The mean fixation time increases exponentially as the fitness gap increases. When type-2 cells are more advantageous than type-1 cells, and when both are less fit than the wild-type, the probability of tunneling is high. Selection is then always against cells of type-1. In this regime the mean fixation time is a decreasing function of the fitness of type-1 cells. As for all escape problems from metastable states, the fixation time scales exponentially with the size of the population. Fixation is noise-driven, and as the population size is increased the noise strength goes down, and hence fixation takes a longer time.

We tested the analytical expressions and numerical results obtained from the WKB approach against individual-based simulations carried out using the Gillespie algorithm. Our theoretical predictions in principle rely on a limit of large but finite populations, and so they can be expected to be valid only for large enough populations. The comparison against simulations demonstrates the accuracy of our theory even at moderate populations of $N = 100$ cells. For populations much smaller than this, the assumptions of the WKB method break down, as the rate-limiting step is then the occurrence of an initial mutant and not the escape from metastable states.

Our results allow an extrapolation to situations when fixation times become very long, for in-

stance for very large populations and/or when mutation rates and fitness parameters are such that selection is against the invading mutants. In these scenarios, stochastic simulations can become too expensive computationally to provide meaningful measurements. Analytical methods based on backward master equation or backward Fokker-Planck equations suffer from computational limitations as well in such cases. The expressions obtained from the WKB approach, on the other hand, remain valid; in fact, they become more accurate as the population size increases.

Our mathematical work complements existing analytical approaches to the Moran model of cells acquiring two successive mutations. Previous work has provided an appropriate machinery with which to compute time-to-fixation of the second mutation in situations without metastable states. The present paper focuses on the opposite situation and specifically addresses cases in which fixation is limited by the escape from long-lived states. This contribution closes a gap in the analytical characterization of fixation and a more complete picture is now available. We have added a new method to the toolbox used to study stochastic tunneling. Our fixed-point analysis provides a systematic procedure to determine which tool to use for a given set of parameters. This accomplishment removes the need for stochastic simulations altogether, or at the very least it limits the circumstances under which they are needed.

The present work has clear limitations in that it focuses on the Moran model with only two successive mutations. Our systematic approach, along with the combined theoretical apparatus of previous work and the WKB approach are, however, readily transferable to more complex models of cancer initiation and progression.

ACKNOWLEDGMENTS

P.A. acknowledges support from the EPSRC and F.M. from the Dana-Farber Cancer Institute Physical Sciences-Oncology Center (NIH U54CA143798).

LITERATURE CITED

Altland, A., A. Fischer, J. Krug, and I. G. Szendro, 2011 Rare events in population genetics: stochastic tunneling in a two-locus model with recombination. Phys. Rev. Lett. **106:** 088101.

Antal, T. and I. Scheuring, 2006 Fixation of strategies for an evolutionary game in finite populations. Bull. Math. Biol. **68:** 1923–1944.

Armitage, P. and R. Doll, 1954 The age distribution of cancer and a multi-stage theory of carcinogenesis. Br. J. Cancer **8:** 8–12.

Assaf, M. and B. Meerson, 2010 Extinction of metastable stochastic populations. Phys. Rev. E **81:** 021116.

Billings, L., L. Mier-Y-Teran-Romero, B. Lindley, and I. B. Schwartz, 2013 Intervention-based stochastic disease eradication. PloS ONE *8*(8)**:** e70211.

Black, A. J. and A. J. McKane, 2011 WKB calculation of an epidemic outbreak distribution. J. Stat. Mech. **2011:** P12006.

Black, A. J., A. Traulsen, and T. Galla, 2012 Mixing times in evolutionary game dynamics. Phys. Rev. Lett. **109:** 028101.

Brillouin, L., 1926 La mécanique ondulatoire de Schrödinger: une méthode générale de résolution par approximations successives. Comptes Rendus de L'Academie des Sciences **183:** 24–26.

Dykman, M. I., I. B. Schwartz, and A. S. Landsman, 2008 Disease extinction in the presence of random vaccination. Phys. Rev. Lett. **101:** 078101.

Ewens, W. J., 2004 *Mathematical Population Genetics. I. Theoretical Introduction* (2nd ed.). Springer-Verlag, New York.

Fisher, J. C., 1958 Multiple-mutation theory of carcinogenesis. Nature **181:** 651–652.

Gatenby, R. A. and T. L. Vincent, 2003 An evolutionary model of carcinogenesis. Cancer Res. **63:** 6212–6220.

Gillespie, D. T., 1977 Exact stochastic simulation of coupled chemical reactions. J. Phys. Chem. **81:** 2340–2361.

Gottesman, O. and B. Meerson, 2012 Multiple extinction routes in stochastic population models. Phys. Rev. E **85:** 021140.

Haeno, H., R. L. Levine, D. G. Gilliland, and F. Michor, 2009 A progenitor cell origin of myeloid malignancies. Proc. Natl. Acad. Sci. U.S.A. **106:** 16616–16621.

Haeno, H., Y. E. Maruvka, Y. Iwasa, and F. Michor, 2013 Stochastic tunneling of two mutations in a population of cancer cells. PloS ONE *8*(6)**:** e65724.

Iwasa, Y., F. Michor, N. L. Komarova, and M. A. Nowak, 2005 Population genetics of tumor suppressor genes. J. Theor. Biol. *233*(1)**:** 15–23.

Iwasa, Y., F. Michor, and M. A. Nowak, 2004 Stochastic tunnels in evolutionary dynamics. Genetics *166*(3)**:** 1571–1579.

Kamenev, A., 2011 *Field theory of nonequilibrium systems*. Cambridge University Press, Cambridge.

Kamenev, A. and B. Meerson, 2008 Extinction of an infectious disease: A large fluctuation in a nonequilibrium system. Phys. Rev. E **77:** 061107.

Knudson, A. G., 1971 Mutation and cancer: Statistical study of retinoblastoma. Proc. Natl. Acad. Sci. U.S.A. **68:** 820–823.

Komarova, N. L., A. Sengupta, and M. A. Nowak, 2003 Mutation–selection networks of cancer initiation: Tumor suppressor genes and chromosomal instability. J. Theor. Biol. *223*(4)**:** 433–450.

Kramers, H. A., 1926 Wellenmechanik und halbzahlige Quantisierung. Zeitschrift für Physik **39:** 828–840.

Lohmar, I. and B. Meerson, 2011 Switching between phenotypes and population extinction. Phys. Rev. E **84:** 051901.

Lynch, M., 2010 Scaling expectations for the time to establishment of complex adaptations. Proc. Natl. Acad. Sci. U.S.A. **107:** 16577–16582.

Michor, F., Y. Iwasa, and M. A. Nowak, 2004 Dynamics of cancer progression. Nat. Rev. Cancer *4*(3)**:** 197–205.

Mobilia, M., 2010 Oscillatory dynamics in rock–paper–scissors games with mutations. J. Theor. Biol. *264*(1)**:** 1–10.

Moolgavkar, S. H., 1978 The multistage theory of carcinogenesis and the age distribution of cancer in man. J. Natl. Cancer Inst. **61:** 49–52.

Moolgavkar, S. H. and E. G. Luebeck, 1992 Multistage carcinogenesis: Population-based model for colon cancer. J. Natl. Cancer Inst. **84:** 610–618.

Moran, P. A. P., 1962 *The statistical processes of evolutionary theory.* Clarendon Press, Oxford.

Nordling, C. O., 1953 A new theory on the cancer-inducing mechanism. Br. J. Cancer **7:** 68–72.

Nowak, M. A., F. Michor, N. L. Komarova, and Y. Iwasa, 2004 Evolutionary dynamics of tumor suppressor gene inactivation. Proc. Natl. Acad. Sci. U.S.A. **101:** 10635–10638.

Nunney, L., 1999 Lineage selection and the evolution of multistage carcinogenesis. Proc. R. Soc. Lond. B **266:** 493–498.

Proulx, S. R., 2011 The rate of multi-step evolution in Moran and Wright–Fisher populations. Theor. Popul. Biol. *80*(3)**:** 197–207.

Rulands, S., A. Zielinski, and E. Frey, 2013 Global attractors and extinction dynamics of cyclically competing species. Phys. Rev. E **87:** 052710.

van Herwaarden, O. A. and J. Grasman, 1995 Stochastic epidemics: Major outbreaks and the duration of the endemic period. J. Math. Biol. **33:** 581–601.

Van Kampen, N. G., 2007 *Stochastic Processes in Physics and Chemistry* (3rd ed.). Elsevier, Amsterdam.

Weinberg, R. A., 2013 *The Biology of Cancer* (2nd ed.). Garland Science, New York.

Weinreich, D. M. and L. Chao, 2005 Rapid evolutionary escape by large populations from local fitness peaks is likely in nature. Evolution *59*(6)**:** 1175–1182.

Weissman, D. B., M. M. Desai, D. S. Fisher, and M. W. Feldman, 2009 The rate at which asexual populations cross fitness valleys. Theor. Popul. Biol. *75*(4)**:** 286–300.

Weissman, D. B., M. W. Feldman, and D. S. Fisher, 2010 The rate of fitness-valley crossing in sexual populations. Genetics *186*(4)**:** 1389–1410.

Wentzel, G., 1926 Eine Verallgemeinerung der Quantenbedingungen für die Zwecke der Wellenmechanik. Zeitschrift für Physik **38:** 518–529.

APPENDIX A: FIXED POINTS AND STABILITY

From the deterministic equations (3) it can be seen that the state $\vec{x} = (0, 0, 1)$ is a fixed point, i.e. $\dot{x}_i = 0$ at this point for $i = 0, 1, 2$. This is the absorbing state, so this result is rather obvious. Non-trivial fixed points exist away from the absorbing state in some parameter regions.

The stability of a fixed point is determined by the eigenvalues of the Jacobian of the deterministic equations (3). Due to the overall constraint $x_0 + x_1 + x_2 = 1$, the system is effectively two-dimensional. We can write the Jacobian in terms of two variables, x_1 and x_2, as

$$\mathcal{J}(x_1, x_2) = \begin{pmatrix} \partial_{x_1}\dot{x}_1 & \partial_{x_2}\dot{x}_1 \\ \partial_{x_1}\dot{x}_2 & \partial_{x_2}\dot{x}_2 \end{pmatrix}. \tag{A1}$$

Along the 1–2 boundary of the concentration simplex, Eqs. (3) can be expressed in terms of a single variable, x_1. A fixed point, x_1^*, on this boundary satisfies the equations

$$\begin{aligned} \dot{x}_1 &= \big[(1-u_2)r_1 - \overline{r}\big]x_1^* = 0 \\ \dot{x}_2 &= u_2 r_1 x_1^* + (r_2 - \overline{r})(1 - x_1^*) = 0, \end{aligned} \tag{A2}$$

where $\overline{r} = r_1 x_1^* + r_2(1 - x_1^*)$. These equalities are satisfied by the value $x_1^* = 1 - u_2 r_1/(r_1 - r_2)$ (along with $x_2^* = 1 - x_1^*$). The parameter range in which this fixed point exists is determined by the condition $0 < x_1^* < 1$, which we can write as $r_2 < (1-u_2)r_1$. The fixed point on the 1–2 edge therefore exists when type-1 cells have a fitness advantage over type-2 cells, the factor $1 - u_2$ accounts for effects of mutation. Increasing this fitness advantage moves the fixed point towards $x_1 = 1$, or equivalently away from the absorbing state at $x_1 = 0$. For vanishing mutation rate u_2, the fixed point approaches the $x_1 = 1$ state.

Evaluating the eigenvalues of the 2×2 Jacobian in Eq. (A1) at this fixed point, we find that the point is stable if $(1 - u_2)r_1 > (1 - u_1)r_0$, and that it is a saddle if $(1 - u_2)r_1 < (1 - u_1)r_0$. These two cases correspond to Regions I and II in Fig. 2.

A fixed point of Eqs. (3) with $x_0 > 0$ is found as

$$\begin{aligned} x_1^* &= \frac{[(1-u_1)r_0 - r_2]u_1 r_0}{u_2 r_1(r_0 - r_2) + (r_0 - r_1)[(1-u_1)r_0 - r_2]}, \\ x_2^* &= \frac{u_1 u_2 r_0 r_1}{u_2 r_1(r_0 - r_2) + (r_0 - r_1)[(1-u_1)r_0 - r_2]}, \end{aligned} \tag{A3}$$

provided the model parameters satisfy $(1 - u_1)r_0 > (1 - u_2)r_1$ and $(1 - u_1)r_0 > r_2$. The further analysis of the Jacobian (A1) at this point shows that the fixed point is stable whenever it exists.

This is the region of parameter space in which cells with one and two mutations respectively are both less fit than the wild-type. This is the case in Regions II and III in Fig. 2. The fixed point moves closer to $x_0 = 1$ when the fitness advantage of the wild type cells is increased (e.g. by lowering the fitness of type-1 cells, $r_1 \to 0$). Decreasing the mutation rates also moves the fixed point closer to $x_0 = 1$.

APPENDIX B: SOLVING THE QUASI-STATIONARY MASTER EQUATION

In terms of the variable $\vec{x} = \vec{n}/N$, we can write the QSME (6) for $\vec{n} \neq \vec{n}_{abs}$ as

$$0 \approx -\frac{1}{\tau}\psi(\vec{x}) = \sum_{\vec{v}} \left[N w_{\vec{v}} \left(\vec{x} - \frac{\vec{v}}{N} \right) \psi \left(\vec{x} - \frac{\vec{v}}{N} \right) - N w_{\vec{v}}(\vec{x}) \psi(\vec{x}) \right], \tag{B1}$$

where $w_{\vec{v}}(\vec{x}) = T^{\vec{v}}_{N\vec{x}}/N$ and $\psi(\vec{x}) = \pi_{N\vec{x}}$. Substituting the WKB ansatz, Eq. (5), into Eq. (B1) and expanding in powers of N^{-1} we arrive at

$$\begin{aligned} 0 \;\; = \;\; & \sum_{\vec{v}} w_{\vec{v}}(\vec{x}) \left\{ e^{\vec{v}\cdot\vec{\nabla}S(\vec{x})} \left[1 + \frac{1}{N}\vec{v}\cdot\vec{\nabla}S_1(\vec{x}) - \frac{1}{2}\frac{(\vec{v}\cdot\vec{\nabla})^2}{N} S(\vec{x}) \right] - 1 \right\} \\ & - \sum_{\vec{v}} e^{\vec{v}\cdot\vec{\nabla}S(\vec{x})} \frac{\vec{v}\cdot\vec{\nabla}}{N} w_{\vec{v}}(\vec{x}) + \mathcal{O}(N^{-2}), \end{aligned} \tag{B2}$$

where we have ignored the term $\mathcal{O}\big((N\tau)^{-1}\big)$ as this term is smaller than $\mathcal{O}(N^{-2})$ (τ scales as e^N). The leading-order terms of this equation are equivalent to the Hamilton-Jacobi equation,

$$H(\vec{q},\vec{p}) = \sum_{\vec{v}} w_{\vec{v}}(\vec{q}) \left(e^{\vec{v}\cdot\vec{p}} - 1 \right) = 0, \tag{B3}$$

where $\vec{q} = \vec{x}$ is the so-called 'position' variable, and $\vec{p} = \vec{\nabla}_{\vec{q}} S(\vec{q})$ is the so-called 'momentum' variable. This equation is best solved using the method of characteristics, i.e. we look for parametric solutions, $(\vec{q},\vec{p}) = (\vec{q}(t),\vec{p}(t))$. These trajectories fulfill Hamilton's equations,

$$\dot{\vec{q}} = \vec{\nabla}_{\vec{p}} H(\vec{q},\vec{p}), \quad \dot{\vec{p}} = -\vec{\nabla}_{\vec{q}} H(\vec{q},\vec{p}). \tag{B4}$$

They satisfy the principle of least action, and correspond to the most likely path taken in the so-called phase-space, the space spanned by $(\vec{q},\vec{p})$. The Hamilton-Jacobi equation has the trivial solution $\vec{p} = \vec{0}$, which corresponds to the deterministic 'relaxation' trajectory, for which the equation of motion is simply

$$\dot{\vec{q}} = \vec{\nabla}_{\vec{p}} H(\vec{q},\vec{p})\Big|_{\vec{p}=\vec{0}} = \sum_{\vec{v}} \vec{v} w_{\vec{v}}(\vec{q}). \tag{B5}$$

As we are interested in escape from a stable fixed point, we seek the non-trivial 'activation' trajectory, for which $\vec{p}_a(\vec{q}) \neq \vec{0}$ in general. The relevant boundary condition is $\vec{p}_a(\vec{q}^{\,*}) = \vec{0}$, where $\vec{q}^{\,*}$ indicates the fixed point of the deterministic dynamics from which the trajectory emanates.

In one-dimension, i.e. in the case of a single fixed point on the 1–2 boundary (Region I of Fig. 2), the Hamilton-Jacobi equation (B3) can be written as

$$H(q,p) = w_+(q)\left(e^p - 1\right) + w_-(q)\left(e^{-p} - 1\right) = 0, \tag{B6}$$

where $q = x_1$ is the concentration of cells of type 1, $p = S'(q)$, $w_+(q) = T^{2\to1}(q)/N$, and $w_-(q) = T^{1\to2}(q)/N$ (reaction rates as described in Eq. (1)). This equation can be solved to obtain the activation trajectory $p_a(q)$, and hence $S(q)$. We can now substitute $p_a(q)$ into the equation consisting of next-leading-order terms ($\mathcal{O}(N^{-1})$) of Eq. (B2) to find $S_1(q)$. Following this procedure we find

$$S(q) = -\int dq\ \ln\left[\frac{w_+(q)}{w_-(q)}\right], \quad S_1(q) = \frac{1}{2}\ln\left[w_+(q)w_-(q)\right]. \tag{B7}$$

The QSD is now determined up to a normalization factor. The QSD is peaked about the fixed point located at $q^* = x_1^* = 1 - u_2 r_1/(r_1 - r_2)$, see Appendix A. Hence we can expand the QSD (5) about this fixed point such that

$$\psi(q) \approx A\exp\left\{-N\left[S(q^*) + \frac{1}{2}(q-q^*)^2 S''(q^*)\right] - S_1(q^*) - \dots\right\}, \tag{B8}$$

where we have used $S'(q^*) = p_a(q^*) = 0$. Normalizing to unity then determines the coefficient A.

The QSD determined above breaks down when $n_1 \lesssim N^{1/2}$, or equivalently when $q \lesssim N^{-1/2}$, i.e. close to the absorbing state. In this region we consider a recursive solution of Eq. (6) that does not rely on a specific form for the QSD, i.e. we do not use the WKB ansatz (5). We expand Eq. (6) about $n_1 = 0$ to obtain

$$0 = \sum_{v=\pm1} w_v'(0)\left[(n_1 - v)\pi_{n_1 - v} - n_1\pi_{n_1}\right]. \tag{B9}$$

This is to be solved for π_{n_1} ($1 < n_1 \lesssim N^{1/2}$). Using $w_-'(0) = 1$, we can write this as

$$f_{n_1+1} = \left[1 + w_+'(0)\right] f_{n_1} - w_+'(0) f_{n_1 - 1}, \tag{B10}$$

where $f_{n_1} = n_1\pi_{n_1}$. This recursive system can be solved to arrive at

$$\pi_{n_1} = \frac{\pi_1\{1 - [w_+'(0)]^{n_1}\}}{n_1[1 - w_+'(0)]} \simeq \frac{\pi_1[w_+'(0)]^{n_1}}{n_1[w_+'(0) - 1]}, \tag{B11}$$

where the second step follows from $w'_+(0) > 1$. Using Eq. (7) and expanding the relevant transition rate, $T^{\vec{v}}_{\vec{n}_{\rm abs}-\vec{v}} = T^{1\to 2}_{(0,1,N-1)}$, about $n_1 = 0$ we can write $\pi_1 \simeq \frac{1}{\tau}$. By matching the recursively obtained boundary-layer solution of Eq. (B11) with the WKB solution in Eq. (B8) at $0 < q \lesssim N^{-1/2}$, we obtain an expression for the fixation time τ, as shown in Eq. (8).

APPENDIX C: NUMERICAL SOLUTIONS FOR FIXATION TIME

We now address the case in which there is an internal stable fixed point of the deterministic dynamics. The problem then retains two degrees of freedom. We follow the initial steps of Appendix B to arrive at the Hamilton-Jacobi equation (B3). Given that the original system is two-dimensional we now find four variables for the Hamilton-Jacobi problem, two position variables q_1 and q_2 (equivalent to x_1 and x_2), and two corresponding momenta p_1 and p_2. These are defined by $\vec{p} = \vec{\nabla}_{\vec{q}} S(\vec{q})$. As the 'energy' is fixed ($H = 0$) we have three effective degrees-of-freedom and no obvious solution to $H(\vec{q}, \vec{p}) = 0$. We consider again Hamilton's equations (B4). These equations describe the trajectory that minimizes the action, and hence by solving these we can then determine the fixation time. To determine the boundary conditions we need to find the fixed points of Eqs. (B4). We first note that there are three zero-momentum fixed points, which correspond to the fixed points of the deterministic equations (3). Following Gottesman and Meerson (2012), we label these as M_1 for the absorbing state ($\vec{q} = (0, 0, 1)$), M_2 for the 1–2 boundary fixed point, and M_3 for the reactive stable fixed point defined by Eq. (A3). As we seek to determine the activation trajectory, we need to find fixed points of Eqs. (B4) with non-zero momenta, but with positions corresponding to M_1 and M_2 (the possible end points of the trajectories). These so-called 'fluctuational fixed points' are labeled as F_1 and F_2.

The relevant trajectory is then found using an iterative method to solve the two-boundary problem. Consider the scenario in which the reactive fixed point M_3 is the only fixed point of the deterministic system for x_1 and x_2, other than the absorbing state, i.e. for parameters in Region III of Fig. 2. Here the activation trajectory that leads to fixation starts at M_3 and finishes at F_1. To start the iteration, we fix the momenta for all times to the values at F_1, and then numerically integrate the equations of motion (B4) for the position vector $\vec{q}$ forward in time, starting at M_3 and keeping the momenta constant. This integration is carried out for a sufficient range of time to reach the vicinity of the fixed point F_1, but not too long to avoid numerical errors building up. In the next step the relations for the momenta in Eq. (B4) are then integrated backward in time using the trajectory $\vec{q}(t)$ found in the previous iteration. The momenta at the start of this backward integration are chosen as those corresponding to F_1. This procedure is then iterated, with alternating forward and backward integration of Hamilton's equation. At each step of the procedure the action of the path is found as

$$S_{31} = \int_0^t dt' \; \vec{p}(t') \cdot \dot{\vec{q}}(t'). \tag{C1}$$

The iteration of alternating forward and backward integration is then repeated until S_{31} has reached convergence. The action can then be used in Eq. (9) to determine the fixation time τ_{31}.

In Region II of parameter space a similar procedure is applied. In this case the minimizing trajectory in $(\vec{p}, \vec{q})$-space which connects M_3 and F_2.